Electrochimica Acta xxx (xxxx) 136063

Contents lists available at ScienceDirect

Electrochimica Acta

journal homepage: http://ees.elsevier.com

Lithium ion storage in 1D and 2D redox active metal-organic frameworks

Jorge Montero [a,b], Daniel Arenas-Esteban [c], David Ávila-Brande [c], Elizabeth Castillo-Martínez [c], Silvia Licoccia [b,**], Javier Carretero-González [a,*]

[a] Institute of Polymer Science and Technology, ICTP-CSIC, Calle Juan de la Cierva 3, 28006, Madrid, Spain
[b] Department of Chemical Science and Technologies, University of Tor Vergata, Via della Ricerca Scientifica, 100133, Rome, Italy
[c] Department of Inorganic Chemistry I, Faculty of Chemistry, Ciudad Universitaria, 28040, Universidad Complutense de Madrid, Spain

ARTICLE INFO

Article history:
Received 19 January 2020
Received in revised form 10 March 2020
Accepted 11 March 2020
Available online xxx

Keywords
Lithium ion batteries
MOF
Energy storage
Tetraoxolene ligand
Electrochemical properties

ABSTRACT

The lithium ion storage properties of a series of metal-organic frameworks (MOFs) with formula {[M(L)(H_2O)$_2$]H_2O}n and [M(CA)(Pyz)]n (where L refers to the tetraoxolene ligands: CA = chloranilate and DHBQ = dihydroxybenzoquinone; Pyz = pyrazine; M = Fe and Mn) and exhibiting a 1D and 2D structure, respectively, have been studied. The 1D MOFs ({[M(L)(H_2O)$_2$]H_2O}n) show higher reversible capacity values for lithium ion insertion with respect to 2D structures containing two organic ligands (M(CA)(Pyz)]n). The gravimetric capacity for the 1D Fe-CA MOF is 75 mAh/g at 2.16 mA/g (~ 1 lithium atom per formula unit) higher than for the Mn complexes which is 65 mAh/g at 2.12 mA/g, though isostructural. Lithium ion insertion in the 1D Mn-CA chains takes place at 2.4 V vs. Li^+/Li which is ~700 mV higher than what is recorded for the Fe analogue. This result is most probably due to much more stable d^5 electronic configuration of Mn^{2+} than d^6 of Fe^{2+} in its isostructural Fe-based framework analogue. The 1D Fe-DHBQ capacity is higher than its manganese analogue 75 mAh/g at 2.5 mA/g (0.8 lithiums) against 40 mAh/g. In general, the high voltages of reaction in these 1D MOFs suggest that they involve the participation of the ligand on the redox processes along with the reduction of the transition metal if any. In fact, the potential of ion insertion changed depending on the metal. This fact along with the absence of evidence of conversion reaction by x-ray diffraction of cycled electrodes suggests that the charge delocalization may be all along the metal-ligand molecular framework participating as a whole hybrid unit in the lithium storage.

1. Introduction

The increasing global demand of energy consumption and the fact that 80% of the total energy produced comes from fossil fuels is affecting negatively climate change and human health due to the proliferation of pollutant agents in the atmosphere [1]. Thus, it is urgent to exploit renewable and environmentally friendly energy sources such as solar energy and wind, bringing them into the electric grid, and also boosting the electrification of transport [2]. These low-carbon emission sources are however intermittent, so it is necessary to couple them with energy storage devices characterized by long-time stability, safety and capability to deliver a massive amount of clean electricity [3]. Within this scenario, the development, by using sustainable routes, of inexpensive, non-toxic and efficient battery components, such as electrode and electrolyte materials, is of the utmost importance [4].

Metal organic frameworks (MOFs) are a unique class of porous coordination polymers (CP) comprising inorganic centers connected to organic linkers which results in a high diversity of crystalline structures with novel functional properties [5]. Because of their rich chemistry, MOFs might be potentially used in a wide range of applications such as gas and solvent adsorption, catalysis, molecular and electronic transport, or energy [6]. Despite their promising properties, their application as electrode materials in energy systems has been hindered by their poor electronic conductivity, limited reversible ion insertion into the structure, and by the occurrence of unwanted conversion/displacement reactions [7]. The improvement of the electronic conductivity in MOFs has been overcome either by hybridizing the metal-organic framework with conjugated polymers, by using conjugated organic ligands as electron carriers [8], or by mixing with conducting carbon additives [9]. To prevent a conversion or displacement reaction from occurring, which might increase the polarization in the MOF electrode, researchers have adopted the strategy of choosing early 3d transition metals to stabilize high oxidation states and therefore achieve higher M-O bond stability with respect to charge variations, and to enable long-range electron delocalization [10]. This was the case of the MIL-53 (Fe) series $Fe^{III}OH(bdc)$] (bdc =1,4-benzenedicarboxylate). MIL-53(Fe)·H_2O ($Fe^{III}(OH)_{0.8}F_{0.2}(O_2CC_6H_4CO_2)$]·$H_2O$) was the first ever reported MOF member to reversibly insert Li^+ ions electrochemically [10]. The electrochemical reactivity observed was due to the partial reduction of Fe^{3+} to Fe^{2+} (mixed-valence state) along with the simultaneous insertion of 0.6 Li^+ in the structure per iron atom at a C/40 rate. The experimental capacity value for MIL-53 MOF's is only ~60% of the theoretical value, and the theoretical capacities are lower than 110 mAh·g^{-1}. The main reason for the drop in the experimental capacity values

* Corresponding author.
** Corresponding author.
E-mail addresses: licoccia@uniroma2.it (S. Licoccia); jcarretero@ictp.csic.es (J. Carretero-González)

https://doi.org/10.1016/j.electacta.2020.136063

is the shortage of permanent porosity which hampers the Li-ion insertion numbers of these MOFs, which in turn inhibits the fully reduction of the Fe^{2+} centers. The control of the structural dimensionality of the MOF, beyond the pore size and distribution, has resulted crucial to increase the lithium storage capacity and power capability [11]. For instance, hexagonal pores formed inside a 2D MOF layers made by combining Cu metal centers with anthraquinone dicarboxylate blocks implied that the redox groups were exposed to the internal surface area exhibiting a great endurance upon the uptake of Li-ions [12]. In fact, the capacity loss in this 2D hybrid framework might be very likely due to the insufficient extraction of Li-ions during charge process and not to pore blocking phenomena such as in 3D MOFs such as MIL-53. This was also the first example of a MOF that allows both metal clusters and ligands to independently exhibit redox activity. The decrease of the structural dimensionality in MOFs from 2D to 1D, exhibiting both redox actives metal and organic linkers, has also led the increasing of both the theoretical and experimental gravimetric capacity values. It is worth to highlight the work done by Peng's Cheng group on the synthesis of different 1D MOFs specially the hybrids containing $[M(C_5O_5)(H_2O)_3]_n$ (M = Mn for 1 and Co for 2; $C_5O_5^{2-}$ = croconate dianion) exhibiting well defined redox processes synergistically from both the metal centre and the ligand along with high gravimetric capacity values up to 729 $mAhg^{-1}$, elevated discharging rates to 2 Ag^{-1} and excellent cycling and stability performance during the cycling process [13]. This group has also evidenced that in highly performance 1D MOFs electrodes for lithium ion batteries [14], where metal and ligand redox activities are coexisting, if the 1D chains are linked by weak hydrogen bonds rather than by strong π–π stacking interactions or covalent bonds, the materials allowed to approach their maximum potential capacity and rate capability (faster lithium ion diffusion) without the negative effect of burying active redox sites like in less accessible porous 3D MOF structures.

Particularly interesting to be explored, as electrode material is the case of low dimensionality metal-tetraoxolene complexes as shown in Fig. 1. The tetraoxolene-bridging mode (Fig. 1A) enables the construction of a variety of highly water stable polymer framework containing 1D and 2D building blocks by using simple and environmentally friendly synthesis routes. In these structures the charge might be delocalized over both metal and ligand indistinguishably. These functional hybrid materials have useful electronic and magnetic properties [15,16] so they have revealed to be highly versatile as electroactive compounds and may be used as sustainable electrode materials in Li ion batteries too.

Wrobleski et al. [17] and Kitagawa et al. [18–20] synthesized a series of MOFs with the formula $\{[M(CA)(H_2O)_2]H_2O\}_n$, $[M(CA)(Pyz)]_n$, and $[M(DHBQ)(H_2O)_2]_n$ (M = Fe^{II} and Mn^{II}) (H_2CA = chloranilic acid) (Pyz = pyrazine) (H_2DHBQ = 2,5-dihydroxy-1,4-benzoquinone). The crystal structure of the $\{[M(CA)(H_2O)_2]H_2O\}_n$ MOF consists of 1D M^{II}-CA^{2-} zig-zag chains connected by hydrogen bonds through water molecules (Fig. 1B). The structure corresponding to the MOFs with the two ligands and with formula $[M(CA)(Pyz)]_n$ has a crystalline porous structure that consists of infinite 2D square grid sheets of M^{II} connected by CA^{2-} dianions and pyrazine along the *c* and *b* axes respectively (Fig. 1C). The metal-ligand unit is redox active and the CA^{2-} anion can induce anomalous electrical properties when coupled to the metal ions [18]. Fig. 1D shows the structure of the MOF with formula $[M(DHBQ)(H_2O)_2]_n$ consisting on 1D M^{II}-DHBQ (M = Fe, Mn) chains connected between them by hydrogen bonds made by water molecules coordinated to the metallic centers. This MOF can also exhibit a trans or cis conformation [17,20,21]. The framework shown in Fig. 1D is the trans conformation with the 1D chains running along the *c*-axis. While in the CA-containing MOFs all four oxygen atoms are bonded to transition metals, in the $[M(DHBQ)(H_2O)_2]_n$ only two of the oxygen atoms of the DHBQ ligand are connected to the metal, and the other two –OH are free to react. Actually, DHBQ-based complexes were able to intercalate water molecules and to evidence proton conductivity due to their low-dimensional open porous crystalline structure and chemical reactivity [20].

Inspired by the chemical and structural properties of these class of coordination polymers, we have synthesized a number of MOFs containing either Fe or Mn metals and different aromatic two-fold symmetric ligands with the following formulas: $\{[M(CA)(H_2O)_2]H_2O\}_n$, $[M(CA)(Pyz)]_n$, and $[M(DHBQ)(H_2O)_2]_n$ (M = Fe^{II} and Mn^{II}). We have also characterized their physico-chemical properties and evaluated the impact of the dimensionality of the framework on their electrochemical performance as sustainable electrode materials for Li-ion batteries. Finally, we have evidenced that the charge might be delocalized all along the metal-ligand molecular framework participating as a whole hybrid unit in the lithium storage mechanism.

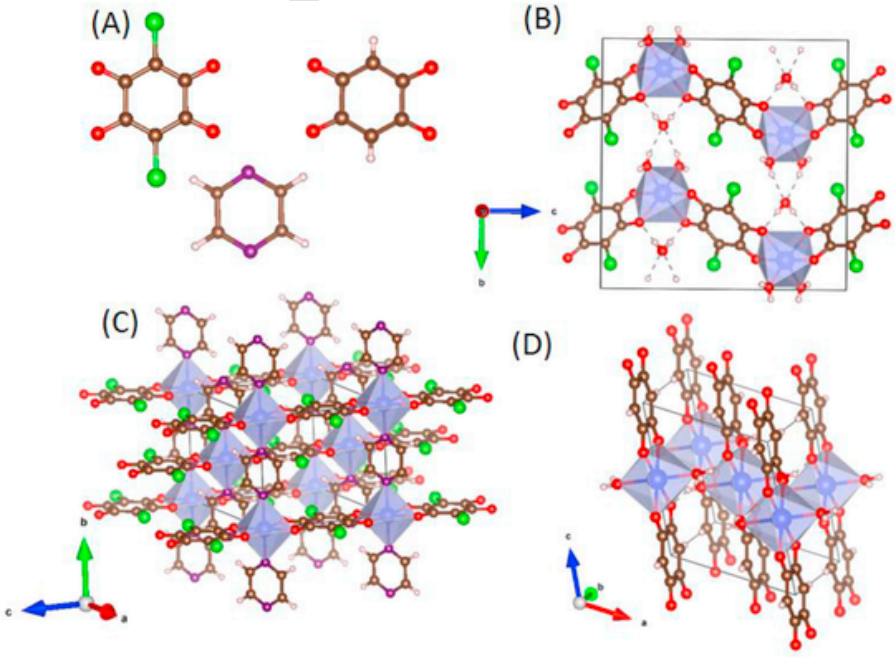

Fig. 1. Chloranilic acid (left), 2,5-dihydroxy-1,4-benzoquinone (right) and pyrazine (down) (A). Structural models of the MOFs $\{[M(CA)(H_2O)_2]H_2O\}_n$ with *C2/c* space group (B), $[M(CA)(Pyz)]_n$ with *C2/m* space group (C) and $[M(DHBQ)(H_2O)_2]_n$ with *C2/c* space group (D). Blue: coordination polyhedra with metal inside, purple: N, red: O, brown: C, white: H, green: Cl. (For interpretation of the references to color in this figure legend, the reader is referred to the Web version of this article.)

2. Experimental section

2.1. MOF synthesis

{[Fe(CA)(H_2O)$_2$]H_2O}$_n$: 83.5 mg of chloranilic acid (0.4 mmol) were dissolved in 60 mL of warm deionized water and then combined with a solution of 111 mg of $FeSO_4{\cdot}9H_2O$ (0.4 mmol) in 20 mL of warm deionized water. Immediately after mixing, dark crystals began to form. After one week crystals were filtered off, washed with water and dried in air. Yield: 93%.

{[Mn(CA)(H_2O)$_2$]H_2O}$_n$: This hybrid complex was prepared following the same procedure than for {[Fe(CA)(H_2O)$_2$]H_2O}$_n$ but with $MnSO_4{\cdot}4H_2O$ as a metal precursor. After one week, crystals were filtered off, washed with water and dried in air. Yield: 60%.

[Fe(CA)(Pyz)]$_n$: For the synthesis of this MOF, 346 mg of $FeSO_4{\cdot}9H_2O$ (1,24 mmol) was added to a refluxing methanol solution (15 mL) containing 100 mg of pyrazine (1.24 mmol). The red-orange iron(II)-pyrazine complex which precipitated was redissolved by adding 1.5 mL of water to the mixture. An aqueous solution of chloranilic acid (260 mg, 1.24 mmol) in water was added to the mix and allowed to cool down to room temperature. After one week the black precipitate was filtered, washed with water and dried in air. Yield: 70%.

[Mn(CA)(Pyz)]$_n$: This MOF was prepared in an analogous way to that of [Fe(CA)(Pyz)]$_n$. After the reaction, a brown precipitate was filtered, washed with water and dried in air. Yield: 50%.

[Fe(DHBQ)(H_2O)$_2$]$_n$: This MOF material was prepared following the same procedure than for {[Fe(CA)(H_2O)$_2$]H_2O}$_n$ but with 2,5-dihydroxy-1,4-benzoquinone as the organic precursor. The black crystals were filtered, washed with water and dried in air. Yield: 80%.

[Mn(DHBQ)(H_2O)$_2$]$_n$: This MOF was prepared following the same procedure than for {[Mn(CA)(H_2O)$_2$]H_2O}$_n$ but with 2,5-dihydroxy-1,4-benzoquinone as the organic linker. The black crystals were filtered, washed with water and dried in air. Yield: 50%

2.2. MOF characterization methods

The content of C, H and N in the coordination complexes was determined by combustion in a LECO CHNS-932 thermal analyzer. The characterization of the content of Fe and Cl in the MOFs materials was carried out by fluorescence with a TXRF EXTRA-II, Rich and Seifert spectrometer. The crystalline structure of the Fe and Mn MOFs was analysed by powder X-ray diffraction (XRD) in the 2θ range of 5°–60° by using a Bruker D8 Advance diffractometer with CuKα radiation (α = 1.54 Å). The chemical functionalities of the coordination polymers were qualitatively analysed by using a FTIR PerkinElmer UATR two on the range of 4000 to 400 cm^{-1}. The thermal stability of the MOFs was evaluated by thermogravimetric analysis (TGA) by using a thermogravimetric balance (model TA Instruments-Q500). The gas used for the analysis was nitrogen for the non-oxidant atmosphere and air for the oxidant atmosphere within a temperature interval of 25 ºC-900 ˚C, at a heating rate of 15 ˚C/min. The average sample mass was 3 mg. The morphology, shape and size of the synthesized MOF particles were studied by high resolution scanning electron microscopy (HRSEM) in a Hitachi S-8000 model with field emission filament and a voltage of 1.0 kV. A comprehensive chemical analysis in the MOFs by using EDS analysis in conjunction with the scanning electron microscopy imaging to confirm the presence of the Fe and Mn in the composition was also carried out.

Electrochemical Measurements. Before the electrochemical study of the lithium storage properties, each MOF material was thermally dried at 70 ˚C under vacuum or at room temperature by using the same vacuum conditions. Then, XRD was performed to determine and choose the conditions where the crystal framework had not changed after drying. Furthermore, the chemical stability of the MOFs in commercial lithium electrolyte was followed inside the glove box before performing the electrochemical tests. For that, 5 mg of each MOF material were placed in a vial and 1 ml of liquid electrolyte was added; then the vial was shacked vigorously and left without disturbing for 3 weeks.

The study of the electrochemical properties of the MOFs was carried out by using stainless steel Swagelok® cells. We employed Kapton® films (25 μm thick) to electrically isolate the inner side of the cells and avoid a short circuit. A disc of lithium metal acted as negative electrode. The active material was mixed by hand with Super P carbon (50 wt%) in an agate mortar. Afterwards, the powder mixture was dried under vacuum at a temperature of 70 ˚C or only under vacuum at room temperature and then transferred to an Argon glove box (MBraun, H_2O < 5 ppm; O_2 < 5 ppm). A porous glass fibre disc (Whatman) acting as a separator was impregnated with 0.2 ml of a commercial electrolyte solution containing a concentration of 1 M of $LiPF_6$ salt in ethyl carbonate (EC) and dimethyl carbonate (DMC) solvents mixture with a 1:1 vol ratio (Sigma-Aldrich). The Li-MOFs half-cells were cycled in a VMP multichannel potentiostat/galvanostat (Bio-Logic) operating at constant current densities (referred as C rates: C/20, C/40 and C/80). See Supplementary File. The cells were cycled in a voltage range between 1.2 and 3.0 V vs Li^+/Li.

3. Results and discussion

3.1. MOF characterization

Elemental analysis of the coordination polymers (Table S1 and Figs. S1-S6)) showed concordance between the theoretical and the experimental content.

Fig. 2 shows the powder X-ray diffraction patterns corresponding to the different MOFs studied herein. The XRD patterns of the MOFs with formula {[Fe(CA)(H_2O)$_2$]H_2O}$_n$ and {[Mn(CA)(H_2O)$_2$]H_2O}$_n$ matched with the bibliographical data published by Kitagawa et al. [18] enclosed on the Cambridge Structural Database (CSD) (Fig. 2A). The MOFs with two different ligands [Fe(CA)(Pyz)]$_n$ and [Mn(CA)(Pyz)]$_n$, were also isostructural to Co^{2+} and Mn^{2+} analogues enclosed on the CSD [19] being the Fe-based MOF phase with this crystal structure herein reported for the first time (Fig. 2B). The XRD pattern corresponding to [Mn(DHBQ)(H_2O)$_2$]$_n$ also matched with the diffractogram published by Yamada et al. [20] (Fig. 2C). However, the coordination polymer with formula [Fe(DHBQ)(H_2O)$_2$]$_n$ showed a completely different XRD pattern that did not fit any of those reported before (Fig. 2D). Abrahams et al. [21] discovered that coordination polymers with formula [M(DHBQ)(H_2O)$_2$]$_n$ (M = Mg or Zn) can adopt a zig-zag structure with cis conformation when the synthesis reaction occurs in a methanol/water solution mixture. These MOFs, when dried in air can change their conformation (unstable) from cis to the linear trans configuration observed by Yamada et al. [20] Therefore, the XRD pattern of the [Fe(DHBQ)(H_2O)$_2$]$_n$, have a different structure than their manganese analogue with trans configuration. Because of the difficulty to growth single crystals for this class of MOF [22] and their chemical instability under the electron beam of the transmission electron microscope, we have not been able to unveil the crystal symmetry with accuracy neither by X-ray nor electron diffraction and confirm their cis or trans configuration or any other different structure. Moreover, the low signal/noise relation value for most of the diffractions and the high x-ray background both most probably due to the x-ray fluorescence also makes difficult the interpretation of the diffractogram corresponding to [Fe(DHBQ)(H_2O)$_2$]$_n$.

The thermal behaviour of the MOFs was studied by TGA in both air and nitrogen atmospheres (Fig. S7) showing slight differences. In air, the MOFs with the formula {[Fe(CA)(H_2O)$_2$]H_2O}$_n$ and {[Mn(CA)(H_2O)$_2$]H_2O}$_n$, both containing 1D chains, show a main weight loss of ~17 wt% approximately at ~120 ˚C and ~150 ˚C respectively. This mass reduction corresponds to the elimination of the three water molecules per formula unit. The slightly higher temperature for this water loss in the {[Mn(CA)(H_2O)$_2$]H_2O}$_n$ framework, suggests that those molecules must be more tightly bonded to manganese than to the more electronegative iron atom. The reason to this fact might be probably due to the higher charge localization in the oxygen-metal bond in the Fe-containing MOF than in the analogue with manganese. A second weight loss for these two MOFs starts at ~300 ˚C that correspond to the beginning of the thermal degradation of the framework, showing a faster decomposition in the Fe-MOF. Under ni-

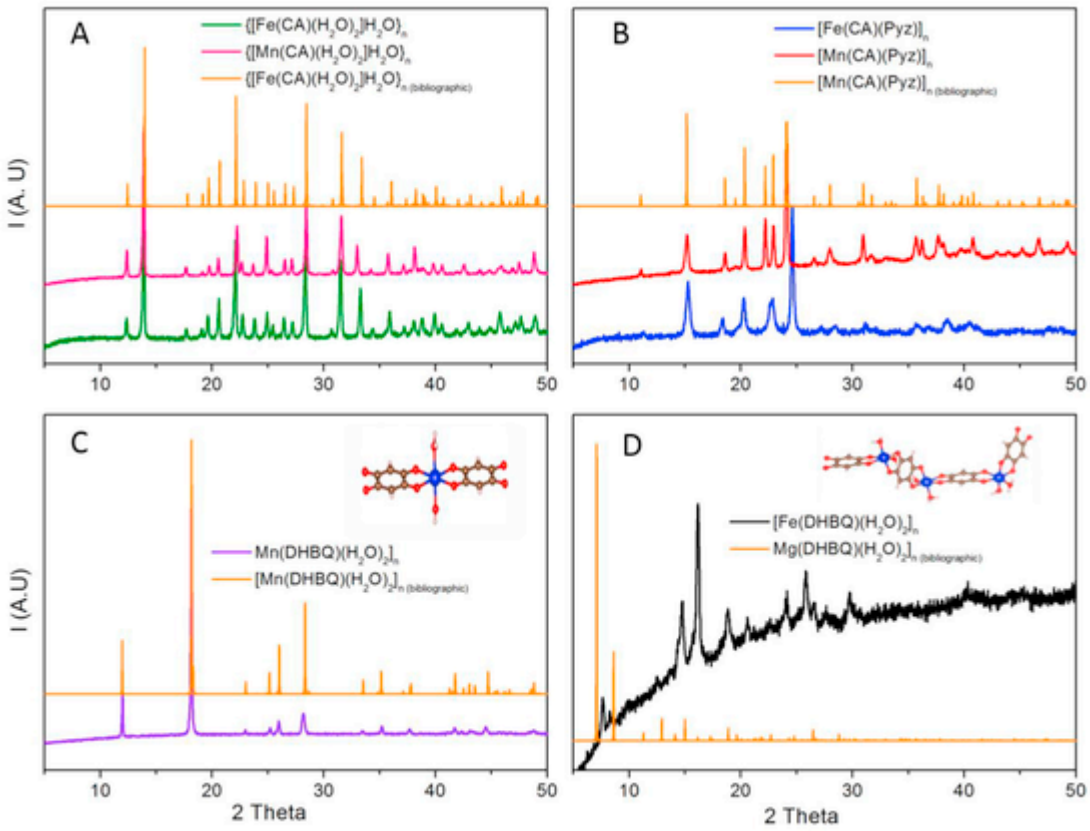

Fig. 2. Comparison between the powder X-ray diffraction patterns of the synthetized MOFs and their bibliographic diffractograms obtained from de CSD for $\{[M(CA)(H_2O)_2]H_2O\}_n$ (A), $[M(CA)(Pyz)]_n$ (B), $[Mn(DHBQ)(H_2O)_2]_n$ (C) and $[Fe(DHBQ)(H_2O)_2]_n$ (D). In the structures on (C) and (D): Blue: M, red: O, brown: C, white: H atoms. (For interpretation of the references to color in this figure legend, the reader is referred to the Web version of this article.)

ing more noticeable in the case of $\{[Fe(CA)(H_2O)_2]H_2O\}_n$. This observation is in agreement with the fact that Fe^{2+} is fastly oxidized into Fe^{3+} in air.

The thermograms in air from the 2D MOFs $[Fe(CA)(Pyz)]_n$ and $[Mn(CA)(Pyz)]_n$ show only one pronounced step of weight loss at ~300 °C and ~400 °C respectively due to their decomposition into the corresponding metal oxides. In nitrogen, the main difference is a shift of the stability of $[Fe(CA)(Pyz)]_n$ up to ~400 °C, due to the higher stability of Fe^{2+} under this atmosphere. Beyond this temperature, the structural collapse occurs gradually in both materials.

In the case of the coordination polymers $[Fe(DHBQ)(H_2O)_2]_n$ and $[Mn(DHBQ)(H_2O)_2]_n$, both thermograms in air and nitrogen show a different behaviour. $[Mn(DHBQ)(H_2O)_2]_n$ exhibits two well defined weight losses, the first one at approximately 100 °C corresponding to the loss of the two water molecules from the framework, and a second ~150 °C in air which is shifted at ~500 °C in nitrogen belonging to the thermal degradation of the coordination polymer.

In the case of $[Fe(DHBQ)(H_2O)_2]_n$, the modification of the shape of the thermograms in both atmospheres is in agreement with the fact that Fe^{2+} is more stable in absence of oxygen. Here it is noticeable a different thermal behaviour of these materials, since they exhibit different crystal structures as it has been demonstrated by X ray powder diffraction.

In view of these results, we can confirm that the hybrid frameworks containing manganese are more thermally stable than their iron counterparts under air atmosphere. In any case, all these degradation temperatures are higher than 60 °C where the decomposition of LP30 begins, so all these MOFs are suitable for the LP30 electrolyte from a thermal stability and safety perspective [23].

As it was mentioned in the experimental section, all the MOF samples were dried in vacuum at 70 °C before the assembly of the electrochemical cells. Subsequently, X-ray diffraction patterns were collected. Only, the crystal structure of $\{[Fe(CA)(H_2O)_2]H_2O\}_n$ is modified after the thermal treatment under vacuum, while the rest of the MOFs retain their parent crystal structure (Figs. S8-S13). Therefore, for this particular material, the electrochemical properties were evaluated only drying under vacuum at room temperature. As discussed before, this stability differences between the $\{[Fe(CA)(H_2O)_2]H_2O\}_n$ and its manganese analogue can be caused by a stronger charge location in the iron-oxygen bond making the water molecules less bonded to the metal center, creating a weaker structure than the $\{[Mn(CA)(H_2O)_2]H_2O\}_n$. Moreover, the most likely to detect thermal transition near the drying temperature were not evidenced by differential scanning calorimetry (DSC) analysis in any of these MOFs, neither during the cooling nor the heating cycle was observed (Fig. S29). Therefore, the structural changes evidenced after thermal treatment under vacuum in the MOF $\{[Fe(CA)(H_2O)_2]H_2O\}_n$ must be might be due to the specific chemical interaction between the Fe and the chloranilic acid.

Fig. 3 shows the IR spectra of the coordination polymers studied herein. The water containing MOFs presented a wide vibration band centred at 3400 cm^{-1} corresponding to the OH group of the water molecules. The strong band at 1500 cm^{-1} corresponding to the C═O vibration was observed in all the MOFs. The band appeared shifted with respect to the pristine vibration band centred at 1600 cm^{-1} corresponding to the carbonyl group in the chloranilic acid and di-hydroxybenzoquinone (Fig. S9) due to the coordination of the ligand with the metal. A band at 1400 cm^{-1} corresponding to the C–N vibration appears in the spectra of $[Fe(CA)(Pyz)]_n$ and $[Mn(CA)(Pyz)]_n$ [24]. For the water containing polymers two more bands at 1300 and 1250 cm^{-1} corresponding to the hydrogen bond between the water molecules and the oxygens from the ligands appeared, although the bands are more intense on the case of the DHBQ containing polymers [25].

The microstructural characterization of the MOFs studied herein has been performed by SEM (Fig. 4). The micrographs show that the hybrid materials $\{[Fe(CA)(H_2O)_2]H_2O\}_n$ and $\{[Mn(CA)(H_2O)_2]H_2O\}_n$ (Fig. 4A and B) share the same lamellar morphology. However, the 2D $[Fe(CA)(Pyz)]_n$ and $[Mn(CA)(Pyz)]_n$ MOFs have different morphology, despite having the same crystal

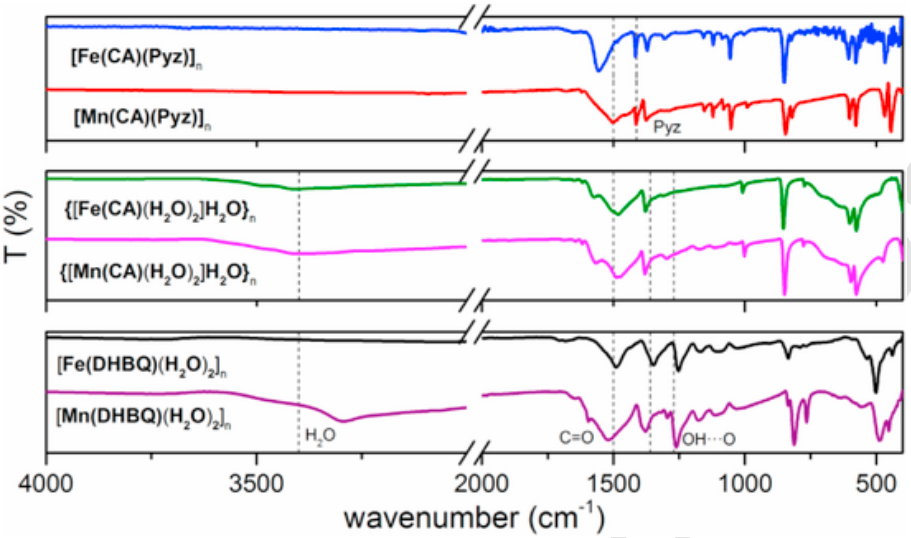

Fig. 3. Infrared spectra of the MOFs studied in this work.

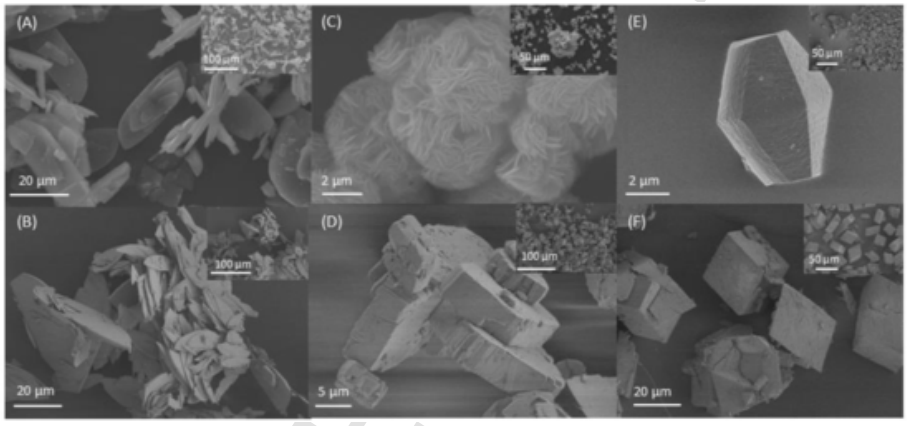

Fig. 4. SEM images of $\{[Fe(CA)(H_2O)_2]H_2O\}_n$ (A), $\{[Mn(CA)(H_2O)_2]H_2O\}_n$ (B) $[Fe(CA)(Pyz)]_n$ (C), $[Mn(CA)(Pyz)]_n$ (D), $\{[Fe(DHBQ)(H_2O)_2]H_2O\}_n$ (E) and $\{[Mn(DHBQ)(H_2O)_2]H_2O\}_n$ (F).

structure. $[Fe(CA)(Pyz)]_n$ had a rose desert morphology (Fig. 4C) while the particles of $[Mn(CA)(Pyz)]_n$ had a tiling shape. This difference on the shape might be a consequence of their different crystallization rates while the crystal nuclei were forming [26]. Experimentally, the $[Mn(CA)(Pyz)]_n$ particles crystallize slowly, yielding large crystals after one day, whereas $[Fe(CA)(Pyz)]_n$ particles crystalize almost immediately after the metalorganic framework is formed. Finally, the SEM micrographs of the $[Fe(DHBQ)(H_2O)_2]n$ and $[Mn(DHBQ)(H_2O)_2]_n$ coordination polymer complexes (see Fig. 4E and F) presented a completely different morphology, having a truncated dodecahedral shape the former and rhombohedral the latter.

3.2. Electrochemical characterization

Before cell assembly, the stability on the electrolyte of the different MOFs was studied (see Fig. S15). The materials $\{[Fe(CA)(H_2O)_2]H_2O\}_n$, $\{[Mn(CA)(H_2O)_2]H_2O\}_n$, $[Fe(DHBQ)(H_2O)_2]_n$ and $[Mn(DHBQ)(H_2O)_2]$ showed an optimum stability in the electrolyte. The suspensions show coloration after several weeks. The $[Fe(CA)(Pyz)]_n$ and $[Mn(CA)(Pyz)]_n$ remained completely stable on the electrolyte during the storage period.

3.2.1. MOFs with CA ligand

The non-thermally treated $\{[Fe(CA)(H_2O)_2]H_2O\}_n$ polymer, (dried only under vacuum at room temperature), shows a plateau at ~1.7 V vs Li^+/Li when cycled at a current density of 2.16 mA/g (Fig. 5A). At that current density, the specific capacity of the battery was 75 mAh/g, despite it was not fully reversible. After 20 cycles at different current densities (Fig. 6A), the capacity of the MOF increased up to 50% more than in the first cycle, achieving a discharge capacity of 40 mAh/g at a current density of 8.64 mA/g. The coulombic efficiency during the initial cycle was ~80% except for the last cycles that exceeds 100% probably due to some anionic insertion [27]. For the $\{[Fe(CA)(H_2O)_2]H_2O\}_n$ thermally treated and dried at 70 °C under vacuum overnight, a smaller plateau was observed at the same potential as the one evidenced in the MOF non-thermally treated. The capacity value achieved by the thermally treated MOF was half (40 mAh/g) of the capacity achieved by the non-thermally treated (75 mAh/g) (Fig. S16). This loss in electrochemical reactivity with respect to lithium ions must be related with the structural transformation suffered when the material was heated (Fig. S8).

The thermally treated $[Fe(CA)(Pyz)]_n$ MOF showed two plateaus at 1.8 V and 1.5 V at a current density of 1.94 mA/g (Fig. 5B). At that same current density, it achieved a specific capacity of 200 mAh/g, the highest of all studied MOFs, although this lithium insertion is not entirely reversible. After 27 cycles at different current densities and different voltage ranges, the capacity of the material at a current density of 7,77 mA/g increase more than a 50%, from a discharge capacity of 20 mAh/g on the first cycles to 45 mAh/g on the last ones (Fig. 6B). The coulombic efficiency started at 50%, scaled up to 80% and then dropped to 30% for cycle 11 and then increased to 100% for the last cycles. The sample cycled without the treatment at 70 °C showed a specific capacity five times smaller than the one heated at the same discharge rate with a capacity, of 40 mAh/g (Fig. S17). This agrees with this MOF retaining its crystal structure upon heating (Fig. S9).

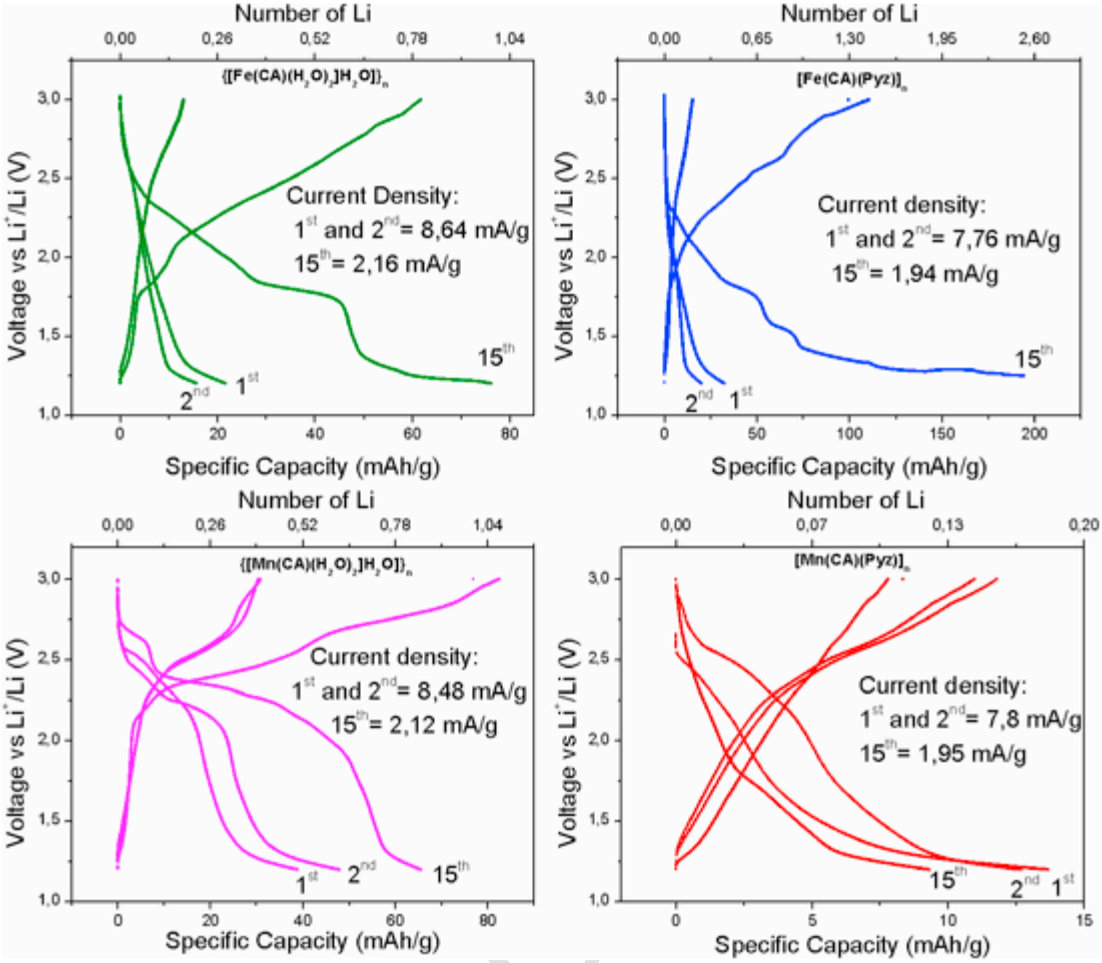

Fig. 5. Galvanostatic discharge-charge profiles of the MOFs with CA and the treatment at 70 °C except for $\{[Fe(CA)(H_2O)_2]H_2O\}_n$ for the cycles 1, 2 and 15.

The thermally treated $\{[Mn(CA)(H_2O)_2]H_2O\}_n$ framework evidenced a plateau at 2.4 V vs Li^+/Li along with a specific reversible capacity of 65 mAh/g at a current density of 2.12 mA/g (C/80) (Fig. 5C). After being cycled at variable current densities the discharge capacity values was between 35 and 40 mAh/g for 8.51 mA/g (C/20) (Fig. 6C). The coulombic efficiency was 60% for the first few cycles and scaled up to 130% for cycle 11 (the first cycle at C/80) and approached 105% for the last cycles. The increase over the 100% might be due to some anionic insertion and/or electrolyte decomposition at that current density. The sample cycled without the treatment at 70 °C showed half the specific capacity of the sample heated at the same discharged capacity (34 mAh/g) (Fig. S18).

For the thermally treated $[Mn(CA)(Pyz)]_n$ framework, no plateau was observed and its specific capacity was only 14 mAh/g at a current density of 1.95 mA/g, the lowest of all the MOFs studied in this work (Fig. 5D). Moreover, despite the reduction on current density, its discharge capacity progressively fell down from 14 mAh/g to 4 mAh/g over 20 cycles (Fig. 6D). The UV–vis results shown (Fig. S28) that the absorbance signal from the supernatant phase corresponding to a dilute suspension of the Mn(CA)(Pyz) in dimethyl carbonate solvent after few days/hours did not change very much, showing practically the same intensity after 15 days. Therefore, this drop in the gravimetric capacity for the Mn(CA)(Pyz) might be most probably due to an irreversible change in the structural-framework of the hybrid material during the electrochemical cycling diminishing the lithium storage properties on it. This change does not necessarily have been related to a change in the crystal structure, and the capacity loss could be due to the insufficient extraction of Li-ions during charge process. Large charge transfer resistance may hinder the movement of Li-ions and prevent some of them from being extracted. The coulombic efficiency of the MOF stayed between 80 and 90% for all of the cycles. For the non-thermally treated $[Mn(CA)(Pyz)]_n$ MOF, the results were similar to the thermally treated (Fig. S19). At a current density of 1.95 mA/g the maximum specific capacity achieved was 10 mAh/g.

In view of these results (Summary of all experimental capacities in Table S2), and if we compare the coordination hybrid materials after the treatment that resulted in the best performance for each of them (thermally or non-thermally treated), we can confirm that the single chain metal-organic structures containing iron and manganese showed higher electroactivity for lithium insertion than their 2D counterparts. The polymer $\{[Mn(CA)(H_2O)_2]H_2O\}_n$ reached a similar capacity than its isostructural iron analogue (65 and 75 mAh/g respectively) but with lithium insertion at a higher average voltage ~ 700 mV. Since both MOFs are isostructural and the only difference is the transition metal, this large voltage difference is due to the transition metal.

In order to draw a valid conclusion about the rate performance and evolution of the gravimetric capacity during the galvanostatic cycling at constant current density, we extended the number of cycles by cycling the cells at one specific rate for the MOFs $\{[Fe(CA)(H_2O)_2]H_2O\}_n$ and $\{[Mn(CA)(H_2O)_2]H_2O\}_n$ (Fig. 7). The results show a progressive increase of the gravimetric capacitance for the Fe-MOF up to 50 cycles and then the value in the next cycles become stable near 70 mAh/g. The behaviour for their isostructural analog Mn-MOF was different as the capacitance value started dropping from value near to 70 mAh/g after 15 cycles approximately. The coulombic efficiency was a bit higher than 100% for the Mn-MOF, most probably due to the electrolyte decomposition during the reduction process while for their Fe-based analog the value was kept near 100%.

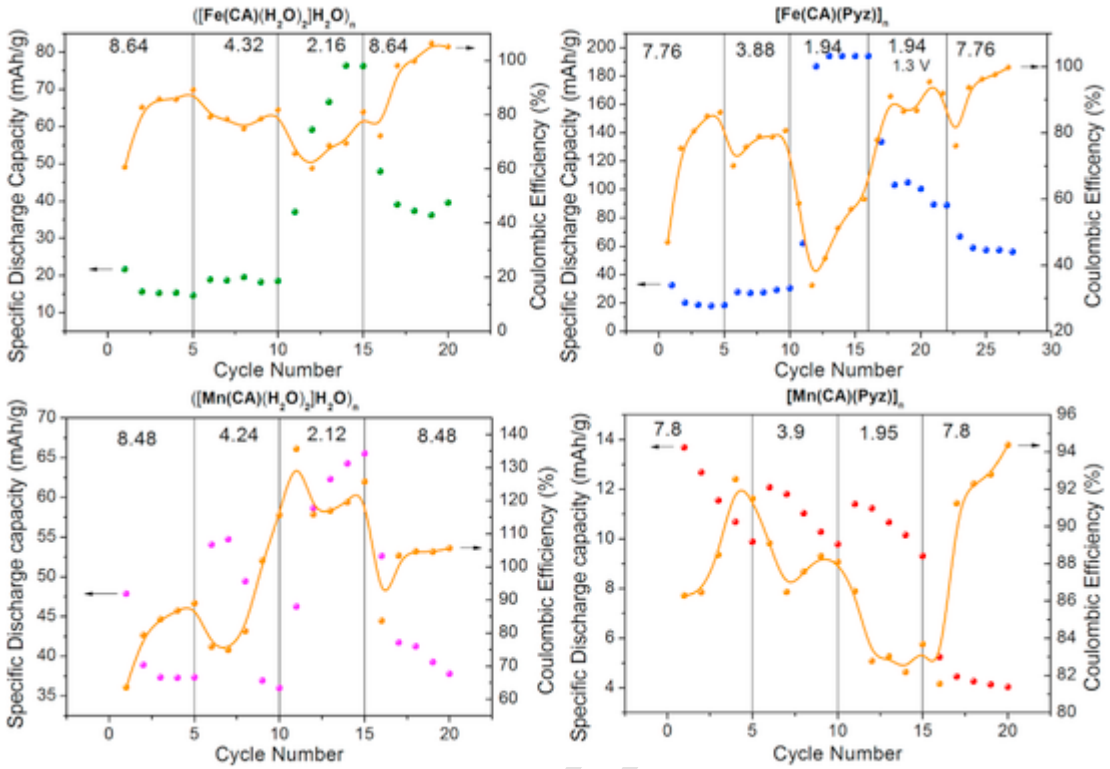

Fig. 6. Rate performance of the MOFs thermally treated at 70 °C (except for {[Fe(CA)(H_2O)2]H_2O}n), at different current densities in mA/g in a voltage range between 1.2 V and 3 V (except cycles 16–22 of [Fe(CA)(Pyz)] which are between 1.3 V and 3 V).

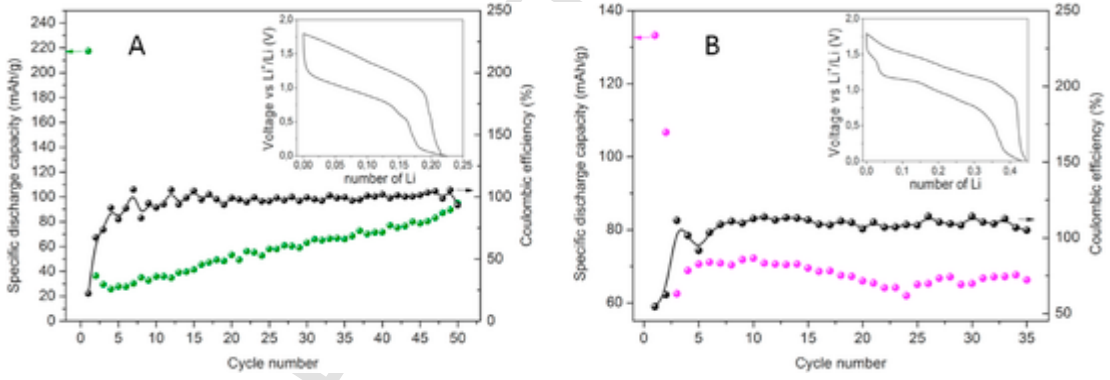

Fig. 7. Galvanostatic performance and coulombic efficiency per 2.12 mA g^{-1} (C/20), for {[Fe(CA)(H_2O)$_2$]H_2O}$_n$ (A) and {[Mn(CA)(H_2O)$_2$]H_2O}$_n$ (B). The inset plot appearing in both graphs corresponds to the cycle number 10.

3.2.2. MOFs with DHBQ ligand

The thermally treated [Fe(DHBQ)(H_2O)$_2$]$_n$ framework evidenced a plateau at ~2.2 V vs Li^+/Li along with a reversible specific capacity of 75 mAh/g at a current density of 2.5 mA/g (Fig. 8A). After 15 cycles at different c-rates the discharge capacity was still increasing. The coulombic efficiency was 30% for the first cycle and stayed between 85 and 100% in the following cycles (Fig. 8B). The non-thermally treated sample showed a specific capacity half of the one thermally treated at the same discharged capacity, 30 mAh/g (Fig. S20). This effect is observed in all the MOFs which crystal structure remained unchanged upon heating, and could be due to the fact that water or solvent adsorbed in the structure was not completely removed when drying only in vacuum.

The non-thermally treated [Mn(DHBQ)(H_2O)$_2$]$_n$ framework evidenced a plateau at ~2 V vs Li^+/Li along with a specific reversible capacity of 40 mAh/g at a current density of 2.5 mA/g (Fig. 8A). After 15 cycles at different c-rates the discharge capacity was still increasing. The coulombic efficiency was 40% for the first cycle and scaled constantly up to 95% for cycle 15 (Fig. 8B). The thermally treated sample showed a similar specific capacity than the non-thermally treated at the same discharged capacity, 30 mAh/g (Fig. S21).

Yielding a snapshot of the voltages of reaction, Fig. 9 shows the d(Q-Q_0)/dV for the coordination polymers studied herein. The {[Fe(CA)(H_2O)$_2$]H_2O}$_n$ polymer (dried only under vacuum and room temperature) plots for the 15th cycle at 2.16 mA/g shows a noticeable reduction process at 1.7 V vs Li^+/Li. Also, smaller plateaus were observed between 2 V and 2.3 V vs Li^+/Li. The {[Mn(CA)(H_2O)$_2$]H_2O}$_n$ framework at a current density of 2.12 mA/g evidenced a pronounced and reversible redox process at 2.4 V vs Li^+/Li. A second redox process appeared at a potential of 2.65 V vs Li^+/Li. [Fe(CA)(Pyz)]$_n$ MOF at 1.94 mA/g showed two pronounced and irreversible processes at 1.8 and 1.5 V vs Li^+/Li. Two other smaller peaks could also be observed a potential of 2 and 2.3 V. For the [Mn(CA)(Pyz)]$_n$ framework at 1.95 mA/g showed two redox processes at 2.5 and 2.3 V vs Li^+/Li. The d(Q-Q_0)/dV graph corresponding to the [Fe(DHBQ)(H_2O)$_2$]$_n$ polymer at 2.5 mA/g had a pronounced and reversible redox process at ~2.2 V vs Li^+/Li. A second and third redox processes

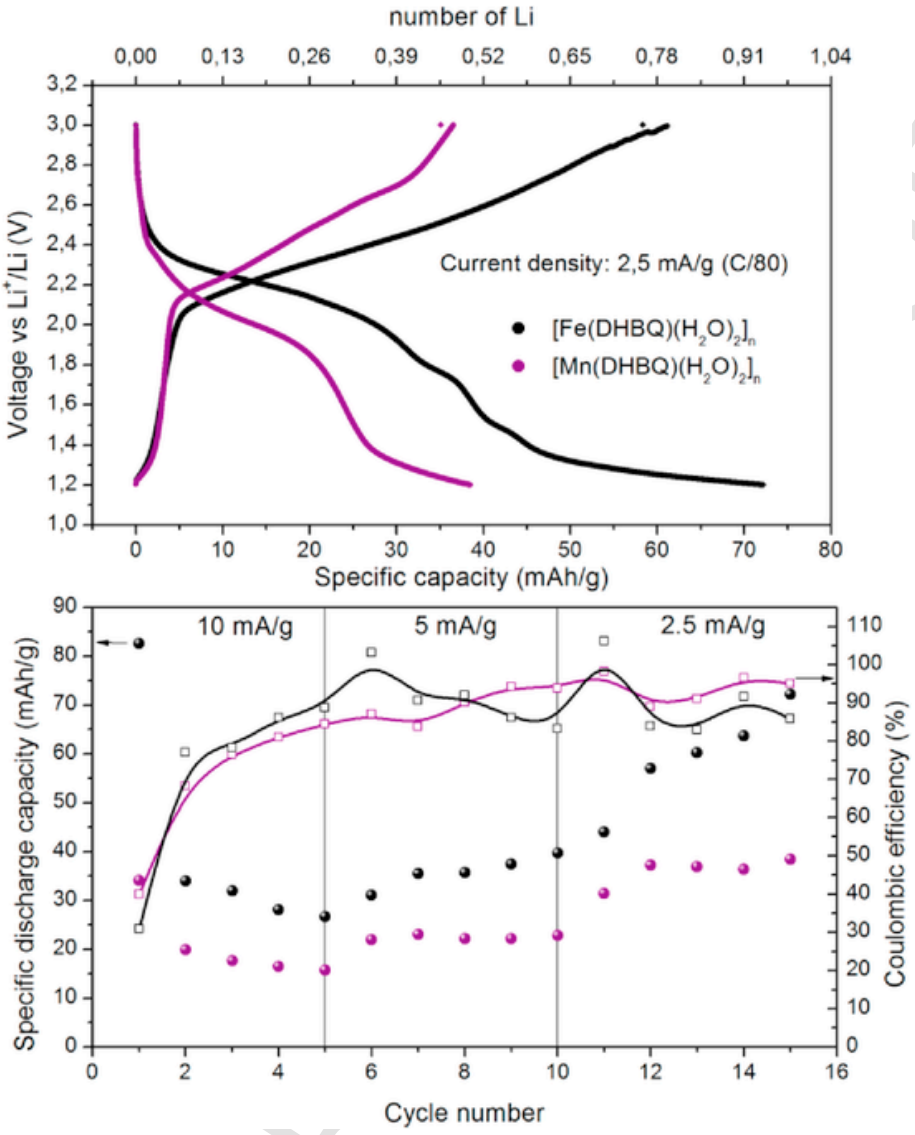

Fig. 8. Galvanostatic discharge-charge profiles (cycle 15) of the MOFs with DHBQ ligand. (up). Rate performance of the MOFs with DHBQ, $[Mn(DHBQ)(H_2O)_2]_n$ (thermally treated at 70 °C), at different current densities at a potential between 1.2 V and 3 V (bottom).

appeared at potentials of 1.4 and 1.8 V similar to the ones found on the other iron containing coordination polymers. The $[Mn(DHBQ)(H_2O)_2]_n$ polymer plot at 2.5 mA/g showed a reduction process at 2 V vs Li^+/Li and a second and third oxidation processes at a potential of 2.4 and 2.6 V.

The observed redox processes could be due to either the reduction of the ligand anion or the reduction of the transition metal (M^{2+}) or both. In transition metal oxides with the transition metal in 2^+ oxidation state (M^{2+}) the oxide anion O^{2-} is fully reduced. The electrochemical reduction can thus only involve reduction of the transition metal, M^{2+}, which typically undergoes a conversion or displacement reaction with the formation of metal nanoparticles, M^0 and lithium oxide [28]. This conversion reaction in TMO occurs around 1 V vs Li^+/Li. In MOFs, the transition metals are coordinated by organic anions, tetraoxolenes in the present work, rather than by oxide anion of the TMO. While the electronegativity of the anion as well as inductive effects in polyanionic anions are known to affect the voltage of reduction of the transition metal, the high voltages of reaction in these MOFs (Fig. 9) suggest that they involve the participation of the ligand on the redox processes, with the aromatic ring and the carbonyl groups along with the reduction of the transition metal if any. In fact, the potential of ion insertion changed depending on the metal. Therefore, it must mean that the metal centre is changing the redox process of the polymers, as it was expected too. For instance, in the chloranilic acid containing MOFs the lithium ion storage capacity and the insertion voltage are higher than those evidenced for the ligand (Fig. S22), which suggest that either the metal centre is the redox active species or the chloranilate ligand is well *hybridized* with the metal centre. Likewise for the DHBQ-based polymers there was an enhancement of the metal-ligand interactions since the voltage of lithium ion insertion occurs at different voltage for the Fe containing coordination polymers than for the manganese analogues. The differences on the lithium insertion potential value must necessarily involve the metal centre of the polymer's structure.

In order to understand the processes occurring while the batteries were discharging we performed an ex-situ XRD analysis at the end of discharge. A series of MOFs batteries with $[Fe(CA)(Pyz)]_n$, $\{[Fe(CA)(H_2O)_2]H_2O\}_n$, $\{[Mn(CA)(H_2O)_2]H_2O\}_n$ and $[Fe(DHBQ)(H_2O)_2]_n$ were assembled and discharged to 1.2 V at a c rate of C/80 (Fig. S23). Next, the batteries were opened inside a glove box and the electrode materials washed, dried and subsequently inserted in a glass capillary tube and then closed hermetically. The capillary tubes were analysed by X-ray diffraction and the patterns were compared with those corresponding to the MOF materials before cycling and those patterns of the metallic iron and manganese species (Figs. S24-S27) in order to identify a possible conversion reaction. The results evidenced that the $[Fe(CA)(Pyz)]_n$ did

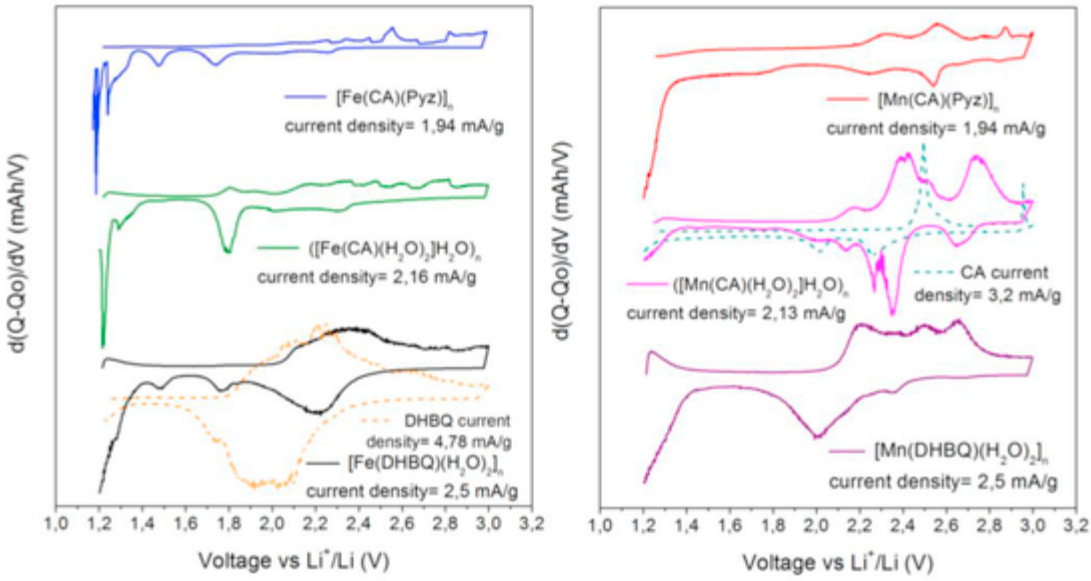

Fig. 9. d(Q-Qo)/dV profiles of the MOFs thermally treated at 70 °C, except for $\{[Fe(CA)(H_2O)_2]H_2O\}_n$ and for $[Mn(DHBQ)(H_2O)_2]_n$ for the cycle 15.

not change its structure during the discharge process, while the MOFs $\{[Fe(CA)(H_2O)2]H_2O\}_n$, $\{[Mn(CA)(H_2O)_2]H_2O\}_n$ and $[Fe(DHBQ)(H_2O)_2]_n$ presented a pattern different from both their non-cycled electrode material and their respective metallic species. These PXRD patterns unveiled that during lithiation only lithium intercalation and not a conversion reaction seems taking place. This lithium insertion hardly affects the crystal structure from $[Fe(CA)(Pyz)]_n$.

Recalling that the large voltage differences observed between Fe-CA and Mn-CA MOFs suggested redox activity coming from the transition metal and considering that no conversion reaction is detected from ex-situ PXRD at the end of discharge, a new scenario opens. This scenario suggests a charge transfer from the transition metal to the ligand during MOF formation, resulting in MOFs where the transition metal is in a higher than 2^+ oxidation state [29]. The $M^{2+\delta}$ would then be reduced during the electrochemical tests herein presented. The fact that the transition metal gets reduced from a mixture of 2^+ and 3^+ to a 2^+ oxidation state, would also be in agreement with the Mn showing higher voltage, since it would reach a much more stable half filled shell d^5 electronic configuration. On the other hand, if reduction from M^{2+} to M^0 occurred, a higher voltage would be expected for the reduction of Fe^{2+} MOF as observed in TMOs and other polyanionic electrode materials [30].

4. Conclusions

We confirm that the single chain metal-organic structures (1D) containing iron and manganese showed higher electroactivity for lithium insertion than their bidimensional (2D) counterparts. The 1D coordination polymer, $\{[Mn(CA)(H_2O)_2]H_2O\}_n$, reached a similar capacity than its isostructural iron analogue (65 and 75 mAh/g respectively) but with lithium insertion at a higher average voltage being appropriate candidates as electrode materials for sustainable Li-ion batteries. We have also evidenced that the thermal treatment performed to the MOF material is crucial to optimize the electrochemical performance of the lithium ion half-cells. For the chlorinate anion containing MOFs the electrochemical capacity values and lithium insertion voltages are higher than those appearing when cycling the ligand alone suggesting a highly *hybridized* coordination polymer structure with superior lithium ion storage properties than the organic ligand alone. Our findings revealed that highly sustainable molecular organic frameworks, prepared by using low-cost precursors and environmentally friendly synthetic routes, are potential candidates to replace the currently expensive, scarce and toxic components contained in the electrode materials of the commercial lithium ion batteries.

Author contributions

J.C.G. supervised the project and conceived the idea. J.M. designed and performed the materials synthesis experiments and characterization with assistance from S.L. and J.C.G.; J.M. and J.C.G. performed the electrochemical characterization experiments. D.A.E. performed the SEM studies. D.A.B. and E.C.M. performed the analysis of the X-ray diffraction data. J.M. and J.C.G. wrote the manuscript with input from all co-authors.

Declaration of interests

The authors declare that they have no known competing financial interests or personal relationships that could have appeared to influence the work reported in this paper.

Acknowledgment

J.M. greatly acknowledge the Funds of his doctoral grant, Materials for Health, Environment and Energy, from the University of Rome Tor Vergata (Italy). E.C.M. acknowledges financial support through a H2020 Marie Skłodowska Curie Individual Fellowship (H2020-MSCA-IF-2016 747449). J.C.G. acknowledges the Ramon y Cajal contract (RYC-2015-17722). J.C.G., D.A.B. and E.C.M. also acknowledges the Retos Projects from MICINN (MAT2017-86796-R, MAT2017-84385-R and RTI2018-094550-A-I00).

Appendix A. Supplementary data

Supplementary data to this article can be found online at https://doi.org/10.1016/j.electacta.2020.136063.

References

[1] EUROPEAN COMMISSION Climate Action Annual Conference of Parties (COP) at COP21 at Stade de France (Gate E) in Paris (7–8 Decemberhttp://ec.europa.eu/clima/policies/international/negotiations/paris/index_en.htm2015
[2] S Chu, Y Cui, N Liu, The path towards sustainable energy, Nat. Mater. 16 (2017) 16–22.
[3] P Leung, A A Shah, L Sanz, C Flox, J R Morante, Q Xu, M R Mohamed, C Ponce de León, F C Walsh, Recent developments in organic redox flow batteries: a critical review, J. Power Sources 360 (2017) 243–283.
[4] D Larcher, J M Tarascon, Towards greener and more sustainable batteries for electrical energy storage, Nat. Chem. 7 (2015) 19–29.
[5] P Kumar, K Vellingiri, K H Kim, R Brown, M J Manos, Modern progress in metal-organic frameworks and their composites for diverse applications, Microporous Mesoporous Mater. 253 (2017) 251–265.

[6] H Zang, J Nai, L Yu, X W Lou, Metal-organic-framework-based materials as platforms for renewable energy and environmental applications, Joule 1 (2017) 77–107.
[7] X Li, F Cheng, S Zhang, J Chen, Shape-controlled synthesis and lithium-storage study of metal-organic frameworks Zn_4O(1,3,5-benzenetribenzoate)$_2$, J. Power Sources 160 (2006) 542.
[8] G de Combarieu, M Morcrette, F Millange, N Guillou, J Cabana, C P Grey, I Margiolaki, G Férey, J-M Tarascon, Influence of the benzoquinone sorption on the structure and electrochemical performance of the MIL-53(Fe) hybrid porous material in a lithium-ion battery, Chem. Mater. 21 (2009) 1602–1611.
[9] Y Mao, Y Guo, Z Li, C Liang, X Peng, Z Lin, Foldable interpenetrated metal-organic frameworks/carbon nanotubes thin film for lithium-sulfur batteries, Nat. Commun. 8 (2017) 14628.
[10] G Férey, F Millange, M Morcrette, C Serre, M Doublet, J Greneche, J M Tarascon, Mixed-valance Li/Fe-based metal-organic frameworks with both reversible redox and sorption properties, Angew. Chem. 119 (2007) 3323–3327.
[11] A E Baumann, D A Burns, B Liu, S Toi, Metal-organic framework functionalization and design strategies for advanced electrochemical energy storage devices, Commun. Chem. 2 (86) (2019) 1–14.
[12] Z Zhang, H Yoshikawa, K Awaga, Monitoring the solid-state electrochemistry of Cu(2,7-AQDC) (AQDC = anthraquinone dicarboxylate) in a lithium battery: coexistence of metal and ligand redox activities in a metal organic framework, J. Am. Chem. Soc. 136 (2014) 16112–16115.
[13] L Zhang, F Cheng, W Shi, J Chen, P Cheng, Transition-metal-triggered high-efficiency lithium ion storage via coordination interactions with redox-active croconate in one-dimensional metal-organic anode materials, ACS Appl. Mater. Interfaces 10 (2018) 6398–6406.
[14] G Li, H Yang, F Li, F Cheng, W Shi, J Chen, P Cheng, A coordination chemistry approach of metal and ligand redox activities in a one-dimensional metal-organic material, Inorg. Chem. 55 (2016) 4935–4940.
[15] B F Abrahams, A T Hudson, L J McCormick, R Robson, Coordination polymers of 2,5-dihydroxybenzoquinone and chloranilic acid with the (10,3)-a topology, Cryst. Growth Des. 11 (2011) 2717–2720.
[16] Y Tuly, C Hendon, K Lomachenko, E Borfecchia, B Melot, M Hudson, J Tarver, M Korzynski, A Stubbs, J Kagan, C Lamberti, C Brown, M Dinca, Reversible capture and release of Cl_2 and Br_2 with a redox-active metal-organic framework, J. Am. Chem. Soc. 139 (2017) 5992–5997.
[17] J T Wroblesky, Brown D B Sythesis, Magnetic susceptibility, and Mossbauer spectra of iron (III) dimers and iron (II) polymers containing 2,5-dihydroxy-1,4-benzoquinones, Inorg. Chem. 18 (1979) 2.
[18] S Kawata, S Kitagawa, H Kumagai, T Ishiyama, K Honda, H Tobita, K Adachi, M Katada, Novel intercalation host system based on transition metal (Fe^{2+}, Co^{2+}, Mn^{2+})-chloranilate coordination polymers. Single crystal structures and properties, Chem. Mater. 10 (1998) 3902–3912.
[19] H Kugamai, S Kawata, S Kitagawa, Fabrication of infinite two-dimensional sheets of tetragonal metal (II) lattices X-ray crystal structures and magnetic properties of $[M(CA)(pyz)]_n$ (M^{2+} = Mn^{2+} and Co^{2+}; H_2CA = chloranilic acid; pyz = pyrazine), Inorganica Chemical Acta 337 (2002) 387–392.
[20] T Yamada, S Morikawa, H Kitagawa, Structures and proton conductivity of one-dimensional M(dhbq)·nH_2O (M= Mg, Mn, Co, Ni, and Zn, H_2(dhbq) = 2,5-dihydroxy-1,4-benzoquinone) promoted by connected hydrogen-bond networks with absorved water, Bull. Chem. Soc. Jpn. 83 (2010) 1.
[21] B F Abrahams, A D Dharma, B Dyett, T A Hudson, H Maynard-Casely, C J Kingbury, L J McCormick, R Robson, A L Sutton, K F White, An indirect generation of 1D M^{II}-2,5-dihydroxybenzoquinone coordination polymers, their structural rearrangements and generation of materials with a high affinity for H_2, CO_2, and CH_4, Dalton Trans. 45 (2016) 1339–1344.
[22] B F Abrahams, K D Lu, B Moubaraki, K S Murray, R Robson, X-ray diffraction and magnetic studies on a series of isostructural divalent metal chloranilates with zigzag polymeric chain structutres and on a dinuclear iron (III) chloranilate, J. Chem. Soc., Dalton Trans. (2000) 1793–1797.
[23] K Xu, Nonaqueous liquid electrolytes for lithium-based rechargeable batteries, Chem. Rev. 104 (2004) 4303–4417.
[24] M Goldstein, W D Unsworth, Infrared and Raman spectra (3500-70 cm^{-1}) and Mossbauer spectra of some pyrazine complexes of stannic halides, Spectrochim. Acta 27A (1971) 1055–1064.
[25] M M Habeeb, H A Al-Wakil, A G Dissouky, N M Rafat, Vibrational spectroscopic studies of hydrogen-bonded complexes between 2,5-dihydroxy-P-benzoquinone and amines, Spectroscopy 15 (2001) 33–44.
[26] J J Richardson, K Liang, F Lisi, M Bjoernmalm, M Faria, J Guo, P Falcaro, Controlling the growth of metal-organic frameworks using different gravitacional-forces, Eur. J. Inorg. Chem. 27 (2016) 4499–4504.
[27] C Jian, Y Fang, W Zhang, X Song, J Lang, L Shi, Y Tang, A multi-ion strategy towards rechargeable sodium-ion full batteries with high working voltage and rate capability, Angew. Chem. Int. 57 (2018) 16370–16374.
[28] P Poizot, S Laurelle, S Grugeon, L Dupont, J M Tarascon, Nano-sized transition-metal oxides as negative-electrode materials for lithium-ion batteries, Nature 407 (2000) 496–499.
[29] Unpublished results.
[30] A Eguia-Barrio, E Castillo-Martinez, X Liu, R Dronskowski, M Armand, T Rojo, Carbodiimides: new materials applied as anode electrodes for sodium and lithium ion batteries, J. Mater. Chem. 4 (2016) 1608–1611.